Approach for improved positioning of an atomic force microscope piezoelectric tube scanner

Md Sohel Rana, Hemanshu R. Pota, Ian R. Petersen

School of Engineering and Information Technology, University of New South Wales, Canberra, ACT 2600, Australia
E-mail: md.rana@student.adfa.edu.au

Published in Micro & Nano Letters; Received on 25th February 2014; Revised on 24th April 2014; Accepted on 13th May 2014

There is a need, in the wide ranging scientific community, to perform fast scans using an atomic force microscope (AFM) with nanoscale accuracy. The performance of an AFM at high scanning speeds is limited because of some serious limitations of its scanning unit; that is, the piezoelectric tube scanner (PTS). To increase the imaging speed of an AFM, a multi-input–multi-output (MIMO) model predictive control scheme is applied in the axes of the PTS to reduce its vibration and cross-coupling effect. The design of this controller is based on an identified MIMO model of the AFM PTS. Moreover, a damping compensator is designed and included in the feedback loop with the plant to suppress the vibration of the PTS at the resonant frequency. Consequently, the proposed controller achieves a higher closed-loop bandwidth, significant damping of the resonant mode of the AFM PTS and results in compensation of the above effects. To evaluate the performance improvement using the proposed control scheme, an experimental comparison of its results with those of the AFM in-built proportional–integral controller is performed. This comparison shows the effectiveness of the proposed controller.

1. Introduction: The atomic force microscope (AFM) is a unique invention of science, which is capable of capturing high-resolution images of samples. It enables precise control, manipulation and interrogation of matter at the nanoscale [1]. It was invented in the early 1980s, and has the ability to generate three-dimensional images of material surfaces at an extremely high resolution down to the atomic level (10^{-10} m) [2]. It is extensively used in various areas such as nanolithography, DNA nanotechnology, optics, microelectronics, material science and nanofabrication [3, 4].

Fast and precise positioning is a basic requirement for nanotechnology applications. Many AFMs use a piezoelectric tube scanner (PTS) for actuation with nanometre resolution in all three spatial directions. Owing to the dynamics of the PTS, the imaging speed of the AFM is limited. The most prominent limitations of the PTS are the low mechanical resonance frequency [5], cross-coupling between the axes [6] and nonlinear behaviour in the form of hysteresis and creep effects [7].

To overcome the above-mentioned limitations of the PTS, control techniques are needed to achieve high-speed AFM imaging. The in-built NT-MDT Ntegra AFM controller is proportional–integral (PI) which achieves good tracking of the reference signal at low scanning speed. However, it suffers at high scanning speed because of the PTS nonlinearities and fails to damp the resonant mode of the PTS, which results in vibrations in a scanned image. To improve the performance of the AFM, different control techniques have been applied for PTS positioning.

Several feedback controllers have been applied to damp the resonant mode of the PTS, such as the positive position feedback (PPF) control in [8] which is a lowpass filter with fast roll-off at high frequencies and high gain at low frequencies. However, because of its lowpass nature, it suffers from the problem of low gain and phase margin.

One of the important problems in AFM imaging is the cross-coupling effect between the axes of its PTS. The cross-coupling effect between the axes of a PTS introduces a significant amount of error in the high-speed precision positioning of the PTS. Owing to this effect, the signal applied to any of the axes of a PTS results in displacements in both axes of the scanner and introduces artefacts on scanned images. To compensate the cross-coupling effect of a PTS in tapping-mode AFM imaging, an inversion-based iterative control method is proposed in [9]. Although this technique works well for cross-coupling compensation, it only produces scanned images up to a scanning speed of 24.4 Hz.

Improved mechanical design of the scanner can also compensate for its cross-coupling effect. In [10], a novel flexure-based piezoelectric stack-actuated *XY* nanopositioning stage is presented, which significantly reduces the cross-coupling effect and combined with integral resonant control and feedforward control techniques, accurate high-speed scans up to 400 Hz were achieved.

Advanced controllers, such as the H^{∞} [11] and iterative learning control [12], have been designed to compensate for the hysteresis effect in an AFM's PTS. In [12], a complex Preisach hysteresis model is used to design a controller to control hysteresis, but the controller produces distortions in scanned images at higher frequencies because it does not take any steps to damp the resonant mode. To compensate for the creep effect, an integrated inversion-based approach is presented in [13].

A single-input–single-output model predictive control (MPC) is examined in [14] which shows a better tracking of the reference signal, but the scanned image has obtained vibration because of the lack of damping in the resonant mode and cross-coupling effects between its axes. To solve these problems, a multi-input–multi-output (MIMO) MPC scheme with a damping compensator is presented in this Letter.

The Letter is organised as follows. Section 2 provides the modelling and identification of the system transfer functions. In Section 3, the control scheme for the AFM scanner is presented. Section 4 reflects the experimental results which illustrate the effectiveness of the proposed control scheme.

2. Identification of the PTS dynamics: In most applications of nanotechnology, speed and precision are important requirements for obtaining good topographical maps of material surfaces using AFMs, many of which use PTS for scanning and positioning at nanometric resolutions. In this work, the PTS is modelled as a two-input–two-output system. A block diagram of the experimental setup is shown in Fig. 1. In this experiment, the plant is identified using a band-limited random noise signal within the frequency range from 10 Hz to 1.0 kHz, using a dual channel HP35665A dynamic signal analyser (DSA). This signal

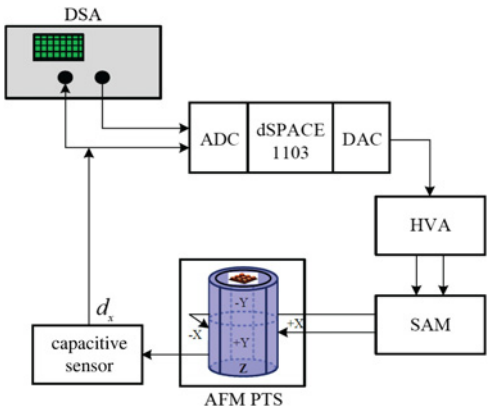

Figure 1 *Block diagram of experimental setup (analogue-to-digital converter and digital-to-analogue converter)*

is supplied to the high-voltage amplifier as an input and the corresponding amplified voltage is supplied to the SAM of the AFM from which there is a direct connection to the PTS. The output displacement of the PTS is taken from the capacitive position sensor. The sensor output is fed back to the DSA to obtain frequency response functions (FRFs). The FRFs generated in the DSA are processed in MATLAB and using the prediction error method, a system model is obtained. The best fit model frequency responses for *X*- and *Y*-piezos are shown in Fig. 2. The two input voltages are applied to the *x*- and *y*-axis amplifiers $[v_x,\ v_y]^{\mathrm{T}}$ while the corresponding output from the capacitive sensors $[d_x,\ d_y]^{\mathrm{T}}$.

The FRFs of the AFM lateral positioning system can be described by the following equation

$$G_{dv}(s) = \begin{bmatrix} \dfrac{d_x(s)}{v_x(s)} & \dfrac{d_x(s)}{v_y(s)} \\ \dfrac{d_y(s)}{v_x(s)} & \dfrac{d_y(s)}{v_y(s)} \end{bmatrix} \tag{1}$$

where (see (2) below)

$$\frac{d_x(s)}{v_y(s)} = \frac{4.242s^3 - 2460s^2 + 2.682 \times 10^6 s - 8.622 \times 10^8}{s^4 + 95.6s^3 + 1.016 \times 10^6 s^2 + 4.498 \times 10^7 s + 2.56 \times 10^{11}} \tag{3}$$

$$\frac{d_y(s)}{v_x(s)} = \frac{0.9309s^3 - 5498s^2 + 2.551 \times 10^6 s - 2.692 \times 10^9}{s^4 + 379.8s^3 + 9.67 \times 10^5 s^2 + 1.772 \times 10^8 s + 2.327 \times 10^{11}} \tag{4}$$

and (see (5) below)

3. Controller design

3.1. Design of damping compensator: This Section presents the design of a damping compensator, the basic structure of which is shown in Fig. 3. Although the MPC controller has itself some damping capacity, a damping compensator is introduced to achieve better damping of the resonant mode and higher bandwidth for an AFM's PTS. The general form of the damping

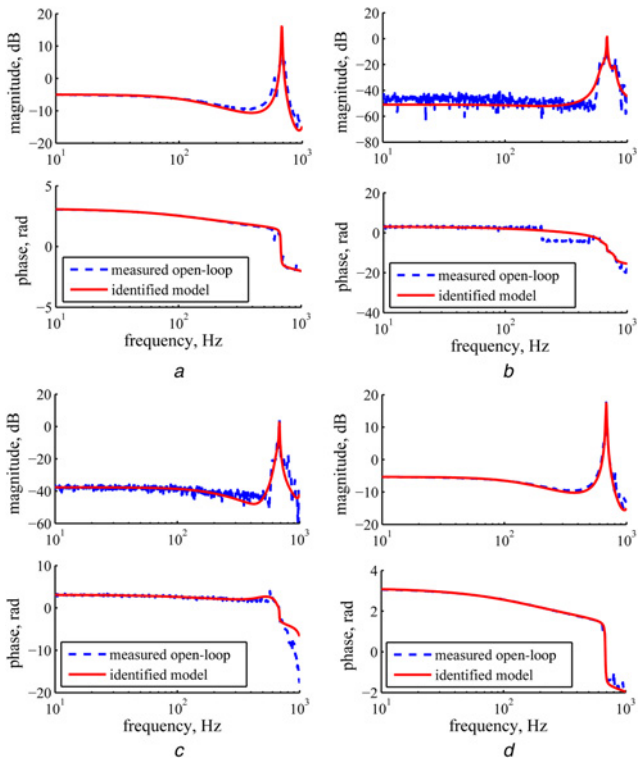

Figure 2 *Frequency responses of the measured and identified systems*
a Input to the *X*-piezo and output from the *X* position sensor
b Input to the *Y*-piezo and output from the *X* position sensor
c Input to the *X*-piezo and output from the *Y* position sensor
d Input to the *Y*-piezo and output from the *Y* position sensor

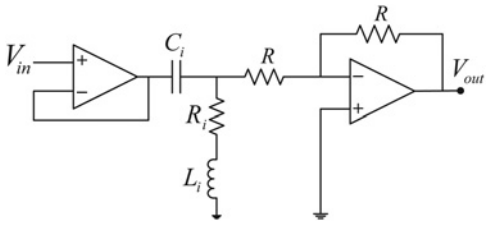

Figure 3 *Structure of the damping compensator*

compensator is

$$A_i = \sum_{i=1}^{N} -k_i \frac{C_i s(R_i + L_i s)}{L_i C_i s^2 + R_i C_i s + 1} \tag{6}$$

where $i = 1, 2, \ldots, N$, k_i is the compensator gain of the corresponding mode. By selecting the proper value of L_i, R_i and C_i, we are able to improve the damping of the resonant mode of the PTS. Since $\omega_i = 1/\sqrt{L_i C_i}$, the value of L_i and C_i are chosen such that ω_i is equal to or almost equal to the resonant frequency of the system.

3.2. Design of MIMO MPC: The purpose of this Section is to present the design of an MIMO MPC controller for minimising

$$\frac{d_x(s)}{v_x(s)} = \frac{-1.197 \times 10^4 s^3 - 2.289 \times 10^6 s^2 + 1.205 \times 10^9 s - 1.599 \times 10^{13}}{s^4 + 3.859 \times 10^5 s^3 + 6.626 \times 10^7 s^2 + 1.806 \times 10^{11} s + 2.849 \times 10^{13}} \tag{2}$$

$$\frac{d_y(s)}{v_y(s)} = \frac{-40.86s^3 + 2.703 \times 10^4 s^2 - 1.363 \times 10^7 s - 6.895 \times 10^{10}}{s^4 + 1.763 \times 10^3 s^3 + 7.812 \times 10^5 s^2 + 8.214 \times 10^8 s + 1.316 \times 10^{11}} \tag{5}$$

doi: 10.1049/mnl.2014.0104

different nonlinearity effects in the AFM PTS. The construction of this closed-loop system is shown in Fig. 4.

Nowadays, MPC is considered to be one of the most widely used multivariable control algorithms in a variety of devices. The MPC scheme is employed to design a tracking controller, the output from which tracks a reference input. It consists of a reference block, a predictor block and an optimiser block. The reference block provides the future reference trajectory, which is used to compute the cost function using the predictions from the predictor block. This cost function is then optimised in the optimiser block. The plant is described by the following state-space model

$$x_m(k+1) = A_m x_m(k) + B_m u(k) \tag{7}$$

$$y(k) = C_m x_m(k) \tag{8}$$

where A_m, B_m and C_m define the discrete state-space plant model, derived from the identified plant model, as stated in (2)–(5) and (6) at a sampling time T_s; $u = [v_x, v_y]^T$ is the manipulated variable or input variable, $y = [d_x, d_y]^T$ is the measured output and x_m is the state variable vector with a dimension of n. To incorporate integral action for disturbance rejection and tracking a reference signal in the MPC algorithm, the plant can be augmented in the following way [15]

$$\overbrace{\begin{bmatrix}\Delta x_m(k+1)\\ y(k+1)\end{bmatrix}}^{x(k+1)} = \overbrace{\begin{bmatrix}A_m & 0\\ C_m A_m & I\end{bmatrix}}^{A}\overbrace{\begin{bmatrix}\Delta x_m(k)\\ y(k)\end{bmatrix}}^{x(k)} + \overbrace{\begin{bmatrix}B_m\\ C_m B_m\end{bmatrix}}^{B}\Delta u(k) \tag{9}$$

$$y(k) = \overbrace{\begin{bmatrix}0 & I\end{bmatrix}}^{C}\overbrace{\begin{bmatrix}\Delta x_m(k)\\ y(k)\end{bmatrix}}^{x(k)} \tag{10}$$

where A, B and C are the augmented system matrices.

The output sequence for N_p, prediction horizon can be written as

$$Y = Fx(k) + \Phi\Delta U \tag{11}$$

in which

$$Y = \begin{bmatrix}y(k+1|k)\\ y(k+2|k)\\ \vdots\\ y(k+N_p|k)\end{bmatrix};\quad \Delta U = \begin{bmatrix}\Delta u(k)\\ \Delta u(k+1)\\ \vdots\\ \Delta u(k+N_c-1)\end{bmatrix}$$

where N_c is the control horizon. The control law is derived based on

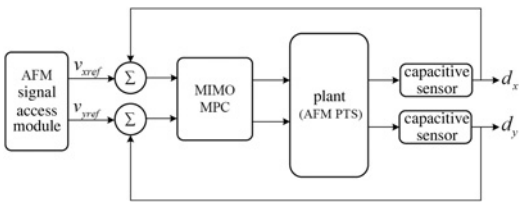

Figure 4 *Block diagram of the closed-loop system*
v_{xref} and v_{yref} are the scanning reference waveforms provided by the AFM signal access module
Outputs d_x and d_y are the displacements of the tube scanner

the minimisation of the cost function defined as

$$J = \sum_{m=1}^{N_p} Q(y(k+m|k) - R_s(k+m))^2 + \sum_{m=1}^{N_c} R(\Delta u(k+m-1))^2 \tag{12}$$

subject to the linear inequality constraints on the system inputs, that is

$$u_{min} \le u(k+i-1) \le u_{max}, \quad i = 1, \ldots, N_c \tag{13a}$$

$$\Delta u_{min} \le \Delta u(k+i-1) \le \Delta u_{max}, \quad i = 1, \ldots, N_c \tag{13b}$$

where Q is the state weighting matrix, R is the control weighting, R_s is the reference signal, u_{min} and u_{max} are the low and high levels of the control action, respectively, and Δu_{min} and Δu_{max} are the low and high levels of the control increments, respectively.

By considering the above equations, the constrained MPC problem can be expressed as a quadratic programming problem

$$\min\left(\frac{1}{2}\Delta U^T E \Delta U + \Delta U^T f\right) \tag{14}$$

s.t.

$$M\Delta U \le \gamma$$

where

$$E = \Phi^T Q \Phi + R$$

$$f = \Phi^T Q F x(k+1|k) - \Phi^T Q R_s$$

$M \in \mathbb{R}^{m_c \times 2N_c}$ and $\gamma \in \mathbb{R}^{2N_c \times 1}$ are computed using (13), m_c is the number of constraints and $R_s \in \mathbb{R}^{2N_p \times 1}$ is the reference signal. A Kalman observer can be used as a state observer and noise filter. It estimates the states from the measured output. The Kalman observer dynamics are

$$\hat{x}(k+1) = (A - LC)\hat{x}(k) + Bu(k) + Ly(k) \tag{15}$$

$$\hat{y}(k) = \hat{C}\hat{x}(k) \tag{16}$$

where $\hat{x}(k)$ is the estimated state, $\hat{y}(k)$ is the estimated output, $\hat{C}$ is the identity matrix of dimensions $n \times n$ and L is the observer gain which depends on the Gaussian white noise, process noise covariance and the measurement noise covariance.

4. Experimental results: For the purpose of performance evaluation, the proposed controller is implemented on the AFM and a frequency-domain analysis is carried out by comparing the measured open-loop and closed-loop frequency responses as shown in Fig. 5. Figs. 5*a* and *d* show comparisons of the closed-loop frequency plots of *X*- and *Y*-piezos obtained by implementing the MIMO MPC controller with the damping compensator, which indicate that it achieves high closed-loop bandwidths of 494 and 503 Hz and 23.28 and 24.88 dB damping of the resonant mode for *X*- and *Y*-piezo, respectively, in turn, significantly reducing vibrations.

The frequency responses for the cross-coupling effects of the AFM PTS are measured and illustrated in Figs. 5*b* and *c*. In open-loop, significant cross-coupling effect can be observed between the lateral axes of the scanner and the effect is higher at and close to the resonance frequency of the PTS. In Fig. 5*b*, it is shown that below the tube resonance frequency, there is approximately 40 dB

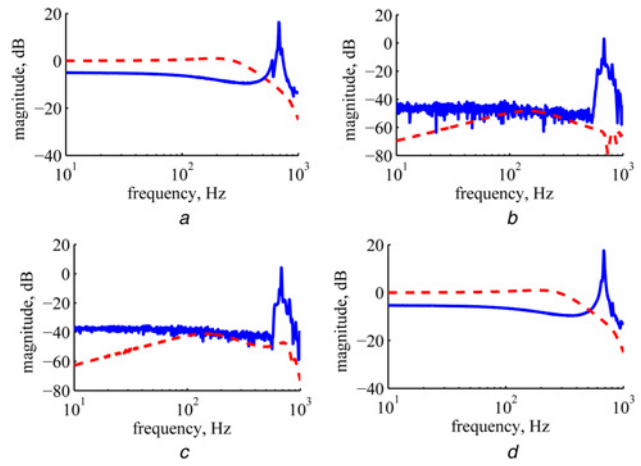

Figure 5 *Comparison of measured open-loop and closed-loop frequency responses*
a Input to the *X*-piezo and output from the *X* position sensor
b Input to the *Y*-piezo and output from the *X* position sensor
c Input to the *X*-piezo and output from the *Y* position sensor
d Input to the *Y*-piezo and output from the *Y* position sensor
Measured open-loop (solid line) and measured closed-loop (dashed line)

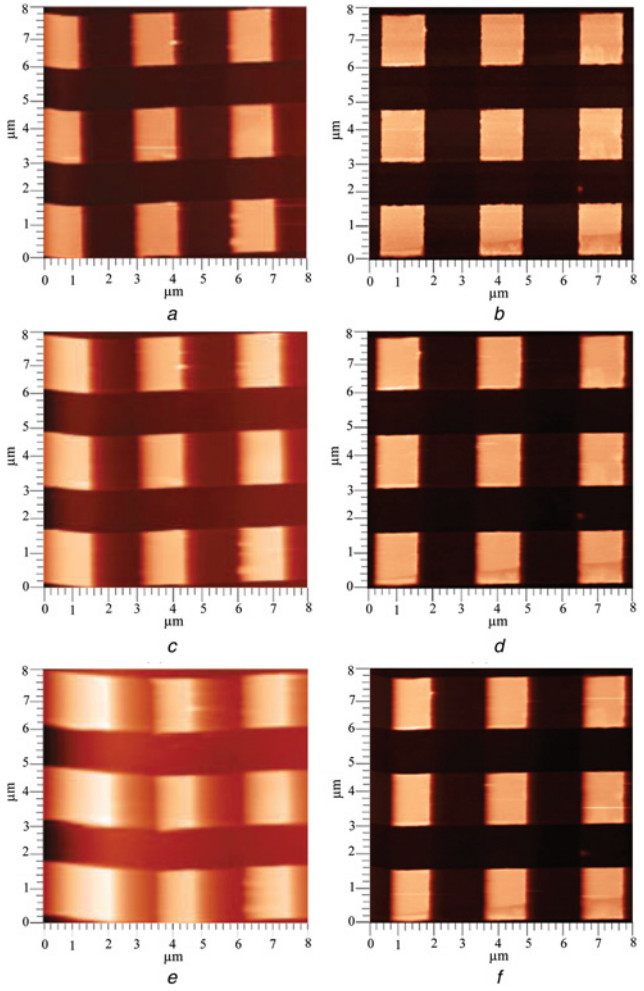

Figure 6 *Compensation of vibration effect at 15.62, 31.25 and 62.50 Hz scanning speeds, Figs. 6a, c, e using the AFM PI controller and Figs. 6b, d, f using the proposed controller*

cross-coupling between the *x*- and the *y*-axis of the scanner at the open-loop condition. This means that an 8 μm amplitude triangular motion of the *x*-axis will translate into approximately 0.08 μm amplitude triangular motion of the *y*-axis. In closed loop, Fig. 5*b* illustrates the substantial decrease in the cross-coupling between the lateral axes of the scanner. In particular, the cross-coupling is about 70 dB. This means that for an 8 μm amplitude triangular motion of the *x*-axis will only translate into approximately 0.002 μm amplitude triangular motion of the *y*-axis.

To demonstrate the effectiveness of the proposed controller to compensate the vibration effect, a comparison of its scanned image with the AFM PI controller is presented in Fig. 6 at 15.62, 31.25 and 62.50 Hz scanning speeds, respectively. The image qualities are nearly the same at 15.62 Hz although the image from the existing PI controller has some roll-off error as shown in Fig. 6*a*. However, at higher frequencies, such as 31.25 and 62.50 Hz, the scanned images using the built-in PI controller have more roll-off error and vibration while those up to 62.50 Hz using the proposed controller retain better quality. To analyse the AFM images, we plot their cross-sectional curves taken in parallel to the square profile of the calibration grating, as shown in Fig. 7. It can be seen that the height profile of the calibration grating is better captured by the proposed controller than by the existing AFM PI controller, resulting in improved images.

The overall improvement in the nanopositioning of the AFM PTS using the proposed controller is clearly seen from Fig. 8, where a suitable comparison is presented between the AFM PI controller and the proposed controller on the basis of the tracking of a triangular signal at 15.62, 31.25 and 62.50 Hz scanning frequencies. Although at a lower scanning speed, the PI controller shows a good tracking of the reference signal but it has become distorted at a higher scanning speed because of the uncontrolled tube resonance as shown in Figs. 8*a*–*c*. Using the proposed controller, we

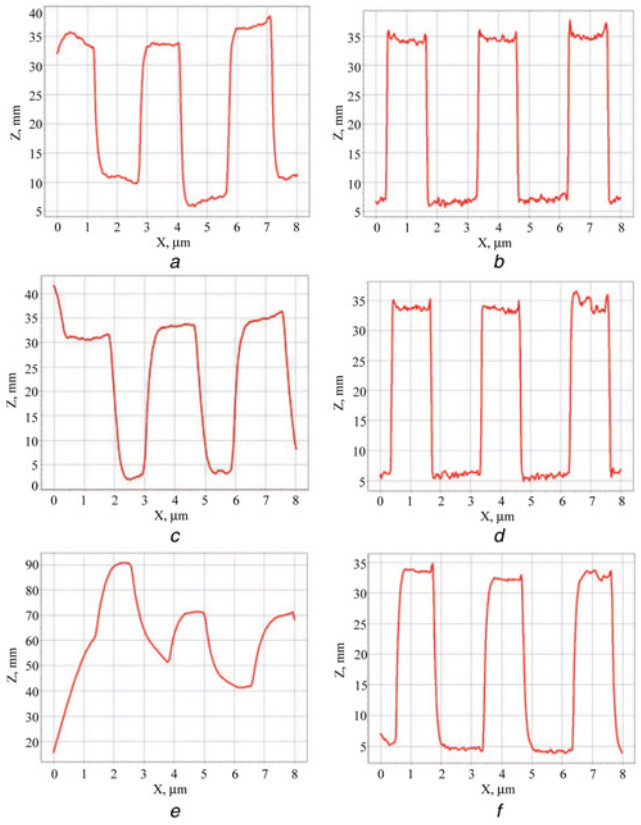

Figure 7 *Z-direction profiles of the sample at 15.62, 31.25 and 62.50 Hz scanning speeds, Figs. 7a, c, e using the AFM PI controller and Figs. 7b, d, f using the proposed controller*

doi: 10.1049/mnl.2014.0104

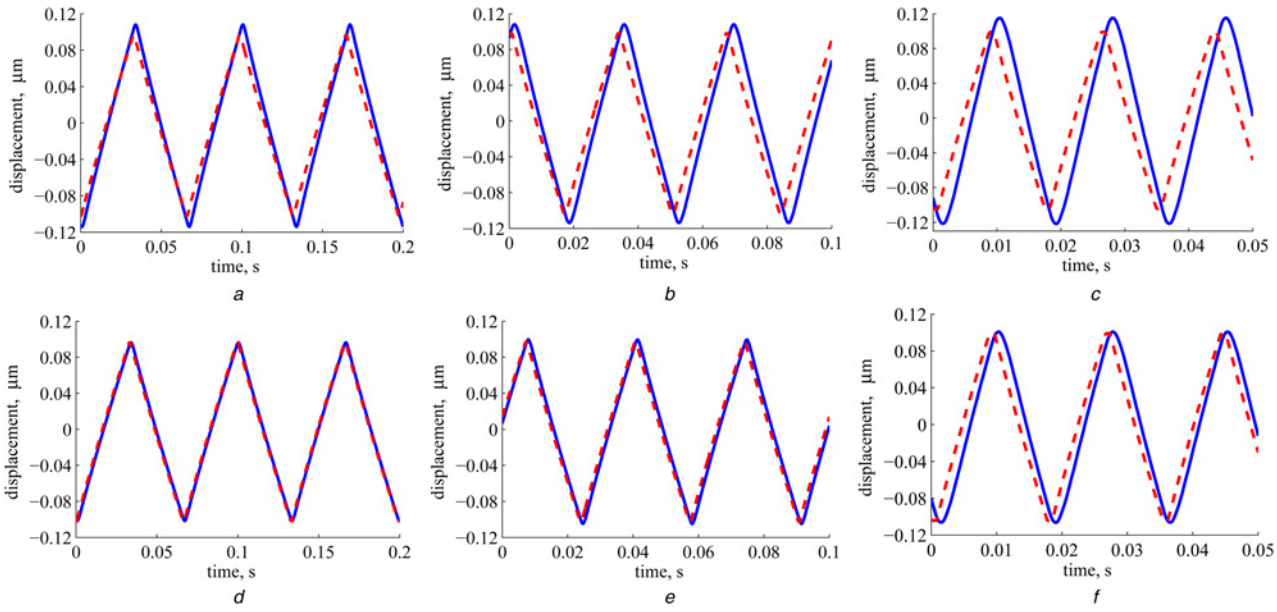

Figure 8 *Figs. 8a–c are those using the AFMPI controller and Figs. 8d–f are those using the proposed controller in the comparison of tracking performance of triangular waves at 15.62, 31.25 and 62.50 Hz, respectively. Reference signal (dashed line), output signal at closed-loop (solid line)*

have obtained a better tracking of the reference signal even at higher frequencies than the AFM PI controller as shown in Figs. 8*d–f*.

5. Conclusion: In this Letter, results from a study of the high-precision positioning of an AFM PTS using an MIMO MPC controller augmented with a damping compensator are reported. The closed-loop frequency-domain performance is compared with the open-loop frequency responses and is shown to achieve significant damping of the resonant mode of the PTSs and vibration and cross-coupling effects between its axes. The experimental results show high-precision tracking and scanning performance of the proposed controller over the AFM PI controller.

6 References

[1] Kenton B.J., Fleming A.J., Leang K.K.: 'Compact ultra-fast vertical nanopositioner for improving scanning probe microscope scan speed', *Rev. Sci. Instrum.*, 2011, **82**, (12), pp. 123703–123703-8

[2] Binnig G.K., Quate C.F., Gerber C.: 'Atomic force microscope (AFM)', *Phys. Rev. Lett.*, 1986, **56**, (9), pp. 930–933

[3] Aphale S., Fleming A.J., Moheimani S.O.R.: 'High speed nano-scale positioning using a piezoelectric tube actuator with active shunt control', *Micro Nano Lett.*, 2007, **2**, (1), pp. 9–12

[4] Rana M.S., Pota H.R., Petersen I.R.: 'High-speed AFM image scanning using observer-based MPC-notch control', *IEEE Trans. Nanotechnol.*, 2013, **12**, (2), pp. 246–254

[5] Moheimani S.O.R., Vautier B.J.G.: 'Resonant control of structural vibration using charge-driven piezoelectric actuators', *IEEE Trans. Control Syst. Technol.*, 2005, **13**, (6), pp. 1021–1035

[6] Tien S., Zou Q., Devasia S.: 'Iterative control of dynamics-coupling-caused errors in piezoscanners during high-speed AFM operation', *IEEE Trans. Control Syst. Technol.*, 2005, **13**, (6), pp. 921–931

[7] Gu G.-Y., Zhu L.-M., Su C.-Y., Ding H.: 'Motion control of piezoelectric positioning stages: modeling, controller design, and experimental evaluation', *IEEE/ASME Trans. Mechatronics*, 2013, **18**, (5), pp. 1459–1471

[8] Mahmood I.A., Moheimani S.O.R.: 'Making a commercial atomic force microscope more accurate and faster using positive position feedback control', *Rev. Sci. Instrum.*, 2009, **80**, (6), pp. 063705–063705-8

[9] Wu Y., Shi J., Su C., Zou Q.: 'A control approach to cross-coupling compensation of piezotube scanners in tapping-mode atomic force microscope imaging', *Rev. Sci. Instrum.*, 2009, **80**, (4), pp. 043709–043710

[10] Yong Y., Aphale S., Moheimani S.O.R.: 'Design, identification, and control of a flexure-based XY stage for fast nanoscale positioning', *IEEE Trans. Nanotechnol.*, 2009, **8**, (1), pp. 46–54

[11] Chuang N., Petersen I.R., Pota H.R.: 'Robust H∞ control in fast atomic force microscopy', *Asian J. Control*, 2013, **15**, (4), pp. 1–15

[12] Leang K.K., Devasia S.: 'Design of hysteresis compensating iterative learning control for piezopositioners: application to atomic force microscopes', *Mechatronics*, 2006, **16**, pp. 141–158

[13] Croft D., Shedd G., Devasia S.: 'Creep, hysteresis, and vibration compensation for piezoactuators: atomic force microscopy application', *Trans. ASME J. Dynamic Syst. Meas. Control*, 2001, **123**, (1), pp. 35–43

[14] Rana M.S., Pota H.R., Petersen I.R.: 'Model predictive control of atomic force microscope for fast image scanning'. IEEE 51st Annual Conf. on Decision and Control (CDC), December 2012, pp. 2477–2482

[15] Wang L.: 'Model predictive control system design and implementation using MATLAB' (Springer, London, UK, 2009)